Hydrogen-Bond Strengthening upon Photoinduced Electron Transfer in Ruthenium-Anthraquinone Dyads Interacting with Hexafluoroisopropanol or Water

*Jihane Hankache, David Hanss, Oliver S. Wenger**

Georg-August-Universität, Institut für Anorganische Chemie, Tammannstrasse 4, D-37077 Göttingen, Germany

oliver.wenger@chemie.uni-goettingen.de

RECEIVED DATE (to be automatically inserted after your manuscript is accepted if required according to the journal that you are submitting your paper to)

ABSTRACT

Quinones play a key role as primary electron acceptors in natural photosynthesis, and their reduction is known to be facilitated by hydrogen bond donors or protonation. In this study, the influence of hydrogen-bond donating solvents on the thermodynamics and kinetics of intramolecular electron transfer between $Ru(bpy)_3^{2+}$ (bpy = 2,2'-bipyridine) and 9,10-anthraquinone redox partners linked together via one up to three *p*-xylene units was investigated. Addition of relatively small amounts of hexafluoroisopropanol to dichloromethane solutions of these rigid rod-like donor-bridge-acceptor molecules is found to accelerate intramolecular $Ru(bpy)_3^{2+}$-to-anthraquinone electron transfer substantially because anthraquinone reduction occurs more easily in presence of the strong hydrogen-

bond donor. Similarly, the rates for intramolecular electron transfer are significantly higher in acetonitrile/water mixtures than in dry acetonitrile. In dichloromethane, an increase in the association constant between hexafluoroisopropanol and anthraquinone by more than one order of magnitude following quinone reduction points to a significant strengthening of the hydrogen bonds between the hydroxyl group of hexafluoroisopropanol and the anthraquinone carbonyl functions. The photoinduced intramolecular long-range electron transfer process thus appears to be followed by proton motion, hence the overall photoinduced reaction may be considered a variant of stepwise proton-coupled electron transfer (PCET) in which substantial proton density (rather than a full proton) is transferred after the electron transfer has occurred.

KEYWORDS: photochemistry, proton-coupled electron transfer, luminescence, cyclic voltammetry, energy transfer

INTRODUCTION

Benzoquinones are textbook examples of organic molecules with strongly pH dependent redox behavior. In bacterial photosynthesis quinone units play a pivotal role as electron acceptors, and in the specific cases of the secondary electron acceptor Q_B and plastoquinone (PQ) the reduction process is accompanied by protonation.[1-2] Both of these electron acceptors are hosted in protein sites in which hydrogen bond donors are present: A serine amino acid residue can form a hydrogen bond to Q_B, while in the case of PQ amino acid residues from a serine and a histidine unit as well as the backbone amide of a phenylalanine unit can act as hydrogen bond donors.[2-3] There have been numerous investigations of photoinduced electron transfer in artificial porphyrin-benzoquinone dyads mimicking the function of the P680 primary donor and the Q_A primary acceptor in biological systems,[4-5] but the influence of hydrogen bond donors on the thermodynamics and kinetics of quinone reduction has received comparatively little

attention in such studies.[6-11,12] The present work provides more insight into the effects of hydrogen bonding on quinone reduction via long-range electron transfer from distant photoreductants.

Due to its favorable photophysical and electrochemical properties, the $Ru(bpy)_3^{2+}$ (bpy = 2,2'-bipyridine) complex represents a popular alternative to porphyrin electron donors.[5, 13] When combined with anthraquinone as an electron acceptor, a comparatively small driving-force for photoinduced electron transfer can be expected.[14-21] We hoped that this fact would render the effect of hydrogen bond formation between solvent molecules (or solvent additives) and the anthraquinone moiety particularly spectacular and easy to observe. As bridging units between the two redox partners we chose *p*-xylenes because they permit the construction of soluble rigid rod-like donor-bridge-acceptor molecules in which fixed-distance electron transfer can be investigated easily. Thus, we prepared a series of three molecules comprised of a $Ru(bpy)_3^{2+}$ electron donor (Ru) and a 9,10-anthraquinone (AQ) moiety linked by one up to three *p*-xylene (xy) spacers (Scheme 1).

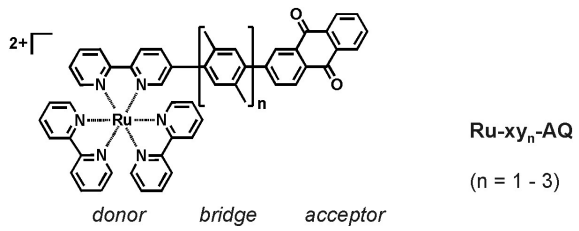

Scheme 1. The three dyads investigated in this work.

Prior work by Gupta and Linschitz provided significant insight into the effects of hydrogen bonding and protonation on the electrochemical behavior of quinones in aprotic solvents.[22] On this basis, our initial investigations (reported in the first two thirds of this paper) focused on the effect of adding increasing amounts of the strong hydrogen-bond donor hexafluoroisopropanol to dichloromethane solutions of our Ru-xy_n-AQ molecules. Because of the special role played by water in biological systems, the present study was extended later to acetonitrile/water solvent mixtures. Evidence for the

influence of water as a hydrogen-bond donor to anthraquinone is discussed in the last third of this article.

RESULTS AND DISCUSSION

Synthesis. Preparation of the molecules from Scheme 1 is based on a previously reported synthetic strategy involving C-C couplings which are accomplished by Suzuki- and Stille-type reactions.[23-25] The most tricky part of the preparative work is the purification of the anthraquinone-(*p*-xylene)$_n$-bipyridine ligands by column chromatography. Detailed synthetic protocols and product characterization data are given in the Supporting Information.

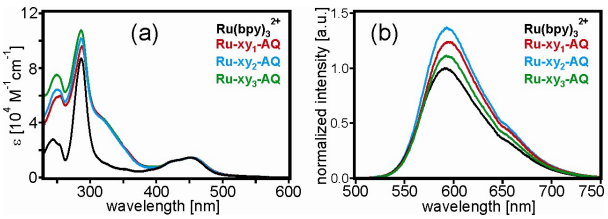

Figure 1. (a) Optical absorption spectra of the Ru(bpy)$_3^{2+}$ reference complex and the three Ru-xy$_n$-AQ dyads from Scheme 1 in acetonitrile solution. (b) Steady-state luminescence spectra of the same compounds in deoxygenated dichloromethane detected after excitation at 450 nm. The color code in panel (b) is the same as in panel (a). The four spectra are normalized to an intensity of 1 (in arbitrary untis) for the Ru(bpy)$_3^{2+}$ reference complex; the data is corrected for differences in absorbance (which was typically between 0.1 and 0.3) at the excitation wavelength.

Photophysical and electrochemical behavior of the Ru-xy$_n$-AQ molecules in pure dichloromethane. Figure 1a shows optical absorption spectra of the Ru-xy$_n$-AQ molecules (n = 1 – 3) and the Ru(bpy)$_3^{2+}$ reference complex in dichloromethane solution. The two most prominent absorption

bands in all four systems are the metal-to-ligand charge transfer (MLCT) band of the $Ru(bpy)_3^{2+}$ unit centered around 450 nm and the bpy-localized π–π* absorption at 290 nm.[26] The UV-Vis spectra of the three donor-bridge-acceptor molecules are nearly identical to each other, there are only minor differences at wavelengths shorter than 265 nm between them. Already in prior investigations we have found that oligo-*p*-xylene bridges yield optical absorption spectra which are substantially less dependent on the length of the molecular bridge than those of dyads with unsubstituted oligo-*p*-phenylene or fluorene bridges,[27-31] a fact that is probably due to a somewhat less significant increase of the overall π-conjugation with increasing bridge length in oligo-*p*-xylenes.

Figure 1b shows the steady-state luminescence spectra of the Ru-xy_n-AQ series (n = 1 – 3) and of $Ru(bpy)_3^{2+}$ in dichloromethane solution (298 K) measured after excitation at 450 nm. The shapes of the four luminescence spectra are essentially identical and are attributed to emission from the lowest ^{3}MLCT excited state of the $Ru(bpy)_3^{2+}$ unit in all four cases. The key observation in Figure 1b is that there is no sign of ^{3}MLCT excited-state quenching by anthraquinone in the Ru-xy_n-AQ dyads in dichloromethane. On the contrary, the emission intensities of the dyads in Figure 1b are even somewhat higher in the dyads than in the reference complex, suggesting that substitution of one of the three bpy ligands with the xylene-anthraquinone units leads to a small increase of the luminescence quantum yield of the ruthenium(II) complex. As will be seen below, this interpretation is consistent with the observation of somewhat slower luminescence decays in the dyads compared to the $Ru(bpy)_3^{2+}$ reference complex (at least in pure CH_2Cl_2).

The cyclic voltammetry data in Figure 2 is useful to understand why there is no sign for $Ru(bpy)_3^{2+}$ ^{3}MLCT excited-state quenching by electron transfer to AQ. The red trace shows the voltammogram of Ru-xy_1-AQ in dichloromethane in presence of tetrabutylammonium hexafluorophosphate ($TBAPF_6$) electrolyte. Oxidation of the $Ru(bpy)_3^{2+}$ complex occurs at a potential of 0.98 V vs. Fc^+/Fc under these conditions, while AQ reduction occurs at -1.35 V vs. Fc^+/Fc; the wave centered around 0 Volts is due to the Fc^+/Fc couple (ferrocene was added to the solutions for referencing). Inspection of Table 1 shows that the Ru(III)/Ru(II) and the AQ/AQ^- reduction potentials of the Ru-xy_1-AQ dyad are similar to those

measured for the individual $Ru(bpy)_3^{2+}$ (0.88 V vs. Fc^+/Fc in CH_3CN) and AQ molecules (-1.32 V vs. Fc^+/Fc in CH_3CN), in line with our expectation of weak electronic interaction between the ruthenium and anthraquinone units over the *p*-xylene bridge.

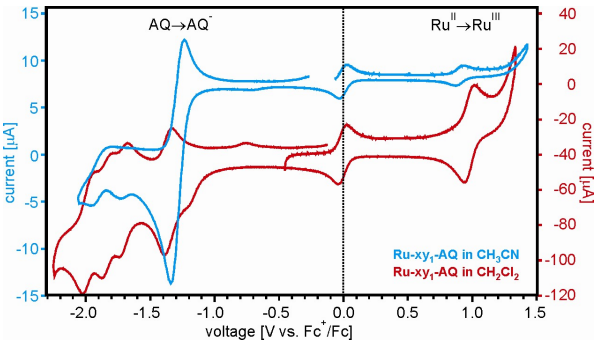

Figure 2. Cyclic voltammograms measured on the Ru-xy_1-AQ dyad in dry and deoxygenated CH_3CN (blue trace) and CH_2Cl_2 (red trace) in presence of 0.1 M tetrabutylammonium hexafluorophosphate ($TBAPF_6$) electrolyte. Traces of ferrocene (Fc) were added for internal voltage calibration; the wave at 0.0 V is due to the Fc^+/Fc couple.

Table 1. Center-to-center donor-acceptor distances (R_{DA}), electrochemical potentials for oxidation of the $Ru(bpy)_3^{2+}$ unit (E_{ox}) and for reduction of the anthraquinone (AQ) moiety (E_{red}), and estimated driving forces (ΔG_{ET}) for photoinduced $Ru(bpy)_3^{2+}$-to-AQ electron transfer.

species	R_{DA} [Å]	E_{ox} [V][a]	E_{red} [V][a]	ΔG_{ET} [eV][d] CH_2Cl_2	ΔG_{ET} [eV][e] CH_3CN	ΔG_{ET} [eV][f] CH_3CN/H_2O
$Ru(bpy)_3^{2+}$		0.88[b]				
AQ			-1.32[b]			
Ru-xy_1-AQ	13.3	0.90[b]/ 0.98[c]	-1.28[b]/ -1.35[c]	0.09	0.03	0.01
Ru-xy_2-AQ	17.6	0.90[b]	-1.29[b]		0.05	0.02
Ru-xy_3-AQ	21.9	0.90[b]	-1.29[b]		0.05	0.03

[a] In units of Volts vs. Fc^+/Fc. [b] In CH_3CN. [c] In CH_2Cl_2. [d] Calculated using eq. 1 and the potentials determined directly in CH_2Cl_2 ($\varepsilon_s = \varepsilon_{ref} = 8.93$). [e] Calculated using eq. 1 and the potentials determined in CH_3CN ($\varepsilon_s = \varepsilon_{ref} = 35.94$). [f] Calculated using eq. 1 and the potentials determined in CH_3CN ($\varepsilon_s = 55.7$,[32] $\varepsilon_{ref} = 35.94$). For all calculations: $E_{00} = 2.12$ eV, r = 4.5 Å. Cyclic voltammograms are shown in Fig. 2 and in the Supporting Information.

Equation 1 is commonly used to estimate Gibb's free energies (ΔG_{ET}) associated with photoinduced electron transfer in donor-bridge-acceptor systems:[33-34]

$$\Delta G_{ET} = e \cdot (E_{ox} - E_{red}) - E_{00} + \frac{e^2}{4 \cdot \pi \cdot \varepsilon_0 \cdot r} \cdot \left(\frac{1}{\varepsilon_s} - \frac{1}{\varepsilon_{ref}} \right) - \frac{e^2}{4 \cdot \pi \cdot \varepsilon_0 \cdot \varepsilon_s \cdot R_{DA}} \qquad \text{(eq. 1)}$$

When applying equation 1 to the Ru-xy_n-AQ molecules, E_{red} and E_{ox} are the electrochemical potentials for anthraquinone reduction and ruthenium oxidation, respectively, while E_{00} is the energy of the photoactive ^{3}MLCT state of the $Ru(bpy)_3^{2+}$ complex (2.12 eV)[26]. ε_0 is the vacuum permittivity, *r* the average radius of the two involved redox partners (assumed to be 4.5 Å), ε_s the dielectric constant of the solvent in which the electrochemical potentials were determined (CH_2Cl_2; 8.93),[35] and ε_r is the dielectric constant of the solvent used for the spectroscopic measurements (CH_2Cl_2; 8.93).[36] Based on molecular models, the center-to-center donor-acceptor distance (R_{DA}) in the Ru-xy_1-AQ molecule is ~13.3 Å. Thus, using equation 1 we estimate that $Ru(bpy)_3^{2+}$-to-AQ electron transfer is endergonic by 0.09 eV in the Ru-xy_1-AQ molecule in dichloromethane (5th column of Table 1), and this may explain the absence of ^{3}MLCT luminescence quenching in this molecule compared to free $Ru(bpy)_3^{2+}$ complex (Figure 1b): It appears that because of its endergonic nature, the photoinduced electron transfer event is not kinetically competitive with other (radiative and nonradiative) ^{3}MLCT relaxation processes. Qualitatively analogous conclusions can be drawn for the longer dyads with n = 2 or n = 3, but as long as experimental data obtained from dichloromethane solutions is concerned, it is useful to restrict the discussion to the Ru-xy_1-AQ molecule.

Hydrogen-bonding between hexafluoroisopropanol and AQ in dichloromethane. As mentioned in the Introduction, Gupta and Linschitz already performed an in-depth study of the effect of hydrogen bonds on the electrochemical behavior of various benzoquinone derivatives, but AQ was not considered in their study.[22] Hexafluoroisopropanol (HFIP; more precisely: 1,1,1,3,3,3-hexafluoro-2-propanol) is known to be a very strong hydrogen-bond donor,[37] but it is not particularly acidic neither in water (pK_a = 9.3) nor in DMSO (pK_a is 17.9).[22] Gupta and Linschitz found that upon addition of HFIP to CH_2Cl_2 solutions of 2,5-dichloro-1,4-benzoquinone or duroquinone the electrochemical potentials for reduction of these two molecules shifted positively, and they attributed this effect to the presence of hydrogen bonds between the hydroxyl group of HFIP and the carbonyl functions of the quinones.[22] Based on this prior work, we anticipated that HFIP would also be able to shift positively the potential for one-electron reduction of AQ through hydrogen-bond donation, and we aimed to explore how strongly this would affect the kinetics of intramolecular $Ru(bpy)_3^{2+}$-to-AQ electron transfer in our dyads in CH_2Cl_2 solution.

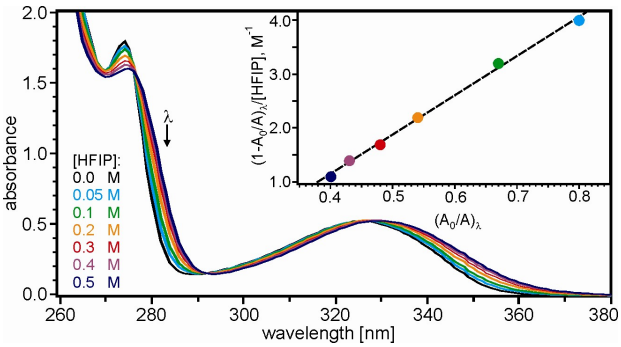

Figure 3. Optical absorption of 9,10-anthraquinone (AQ) in CH_2Cl_2 in presence of increasing concentrations of hexafluoroisopropanol (HFIP); concentration of AQ was 10^{-4} M; concentration of HFIP was as indicated in the legend (color code). The inset shows a plot of the experimental absorbance data at a detection wavelength of 283 nm (marked by the arrow) according to equation 3; the color code in the inset is the same as in the rest of the figure.

In a first step, we searched for experimental evidence for hydrogen bonding between HFIP and charge-neutral AQ. One piece of evidence comes from optical absorption spectroscopy. Figure 3 shows the spectral changes observed in the UV-Vis spectrum of a 10^{-4} M solution of free 9,10-anthraquinone in CH_2Cl_2 following addition of increasing amounts of HFIP. In pure CH_2Cl_2 there is an absorption band maximum at 327 nm which shifts to 332 nm at an HFIP concentration of 0.5 M, whereas the band maximum at 273 nm shifts to 275 nm while at the same time losing intensity. There are well-defined isosbestic points at 277 nm and 292 nm, signaling the presence of only two spectroscopically slightly distinct species. The outcome of the overall HFIP titration in Figure 3 is reminiscent of the spectral changes associated with the addition of 2,4,6-trimethylpyridine to phenol solutions in CCl_4, which were interpreted in terms of hydrogen bonds occurring between the phenol molecules and the pyridine base.[38] Thus it appears plausible to assign the two species observed in the course of the UV-Vis titration of Figure 3 to free AQ and AQ which is accepting a hydrogen bond from HFIP. It appears reasonable to assume that the two species are in chemical equilibrium:

$$\text{AQ} + \text{HFIP} \leftrightarrows \text{AQ-HFIP} \qquad \text{(eq. 2)}$$

Attempts to perform the same titration with any of the Ru-xy$_n$-AQ molecules (rather than free AQ) failed because the AQ absorptions at ~330 nm and ~275 nm have extinction coefficients (~5000 $M^{-1}cm^{-1}$ and ~18000 $M^{-1}cm^{-1}$, respectively; Figure 3),[39] which are significantly lower than those of spectrally overlapping electronic transitions occurring on the $Ru(bpy)_3^{2+}$ unit (the π–π^* absorption around 290 nm has $\varepsilon \approx 10^5$ $M^{-1}cm^{-1}$; Figure 1).[26]

Mataga and Tsuno developed a procedure for quantitative analysis of hydrogen-bonding equilibria using optical absorption data,[38, 40-41] and in equation 3 we adapted their original fit function in order to estimate the equilibrium constant ($K_{eq}^{(AQ)}$) for the chemical equilibrium of equation 2.

$$(1-A_0/A)_\lambda / [\text{HFIP}] = -K_{eq}^{(AQ)} + K_{eq}^{(AQ)} \cdot (\varepsilon_{AQ\text{-}HFIP}/\varepsilon_{AQ})_\lambda \cdot (A_0/A)_\lambda \qquad \text{(eq. 3)}$$

In equation 3, [HFIP] represents the concentration of HFIP, whereas A_0 and A are the absorbance values of AQ in absence and presence of HFIP at a given wavelength λ (at a fixed AQ concentration of 10^{-4} M). $\varepsilon_{AQ\text{-}HFIP}$ and ε_{AQ} are the extinction coefficients of hydrogen-bonded AQ and free AQ at this specific wavelength λ. The inset of Figure 3 shows a plot of $(1\text{-}A_0/A)_\lambda$ / [HFIP] versus $(A_0/A)_\lambda$ for the detection wavelength of 283 nm (marked by an arrow labeled λ in Figure 3). At this wavelength between the two band maxima there are particularly significant changes in absorption upon HFIP addition. A linear regression fit to the data in the inset yields a slope of 7.28 and an intercept of -1.76 (with an R^2-value of 0.9987). Although both the slope and the intercept contain information on the magnitude of $K_{eq}^{(AQ)}$, it is not uncommon to estimate the equilibrium constant directly from the intercept because the extinction coefficient of the hydrogen-bonded molecule (here: $\varepsilon_{AQ\text{-}HFIP}$) is sometimes difficult to determine accurately.[38] From the intercept of our fit we obtain $K_{eq}^{(AQ)}$ = 1.76 M^{-1}. When attempting to extract similar information from the slope, one may use $\varepsilon_{AQ} \approx 3000\ M^{-1}cm^{-1}$ based on the spectrum in Figure 3 at [HFIP] = 0.0 M (black trace) and $\varepsilon_{AQ\text{-}HFIP} \approx 7000\ M^{-1}cm^{-1}$ based on the spectrum at [HFIP] = 0.5 M (purple trace). This procedure yields $K_{eq}^{(AQ)}$ = 3.12 M^{-1}, which is in reasonable agreement with the value obtained from the intercept. Given the uncertainties associated with the determination of equilibrium constants by this method, it appears reasonable to conclude that $K_{eq}^{(AQ)}$ is on the order of 1 M^{-1} for neutral AQ in CH_2Cl_2. We assume that this is not only true for free 9,10-anthraquinone but also for the AQ moiety in the Ru-xy_n-AQ molecules. The order of magnitude found for $K_{eq}^{(AQ)}$ is reasonable in view of other comparable hydrogen-bonded (charge-neutral) systems in aprotic solvents.[42] To name just one specific example, the equilibrium constants for formation of hydrogen-bonded 1:1 adducts between a variety of differently substituted phenol molecules and 2,4,6-trimethylpyridine in CCl_4 range from 2.2 M^{-1} to 82 M^{-1}.[38]

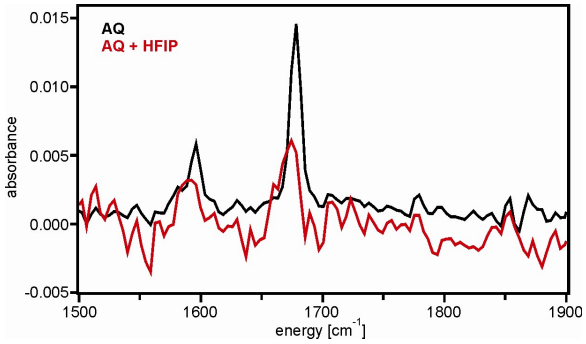

Figure 4. Black trace: Infrared spectrum of a solution of 9,10-anthraquinone (AQ) in CH_2Cl_2 in the spectral region of the carbonyl stretching frequency in absence of HFIP. The red trace was measured on the same solution after addition of a small amount of HFIP.

Figure 4 illustrates our attempts to obtain evidence for hydrogen-bonding between HFIP and AQ using infrared spectroscopy. In agreement with prior studies, we observe the CO stretch of unbound AQ in CH_2Cl_2 at 1678 cm^{-1} (black trace).[43-44] When adding HFIP to the solution, this signal gets weaker and is shifted to lower energies (red trace). Technical difficulties made accurate determination of the HFIP concentration difficult, but we estimate that the final concentration was near 0.1 M. At this point the CO stretch has shifted by -4 cm^{-1}. Even though this shift is very small, we are positive that it is not an instrumental artifact. Changes in dielectric constant may cause shifts of IR frequencies, but in our specific case relatively small amounts of HFIP (0.1 M; $\varepsilon_s = 16.6$)[35] were added. Consequently, it appears possible that the small shift in the CO stretch upon HFIP addition is indeed due to hydrogen bonding. For reference, the CO stretch of ethyl acetate in cyclohexane shifts by -13 cm^{-1} upon addition of 20% of aniline as a hydrogen-bond donor.[45] The AQ concentration in our experiment was near 1 M, and hence the observation of a 4-cm^{-1} shift is quite remarkable and may even suggest that the interaction between HFIP and AQ is stronger than what we have concluded based on the UV-Vis data from Figure 3. However, technical limitations precluded estimation of an association constant from solution IR

experiments, and we note that our $K_{eq}^{(AQ)}$ value determined from optical absorption spectroscopy is in line with hydrogen-bonding equilibrium constants determined in prior studies of comparable systems.[38]

Hydrogen-bonding between hexafluoroisopropanol and $AQ^{\bullet-}$ monoanion in dichloromethane. Figure 5 shows a series of cyclic voltammograms obtained from measurement of Ru-xy_1-AQ in CH_2Cl_2 solution in presence of increasing concentrations of HFIP. Ferrocene was added to the solution for internal referencing, and the prominent reversible wave centered at 0 Volts is due to the Fc^+/Fc couple (dashed vertical line in the middle).

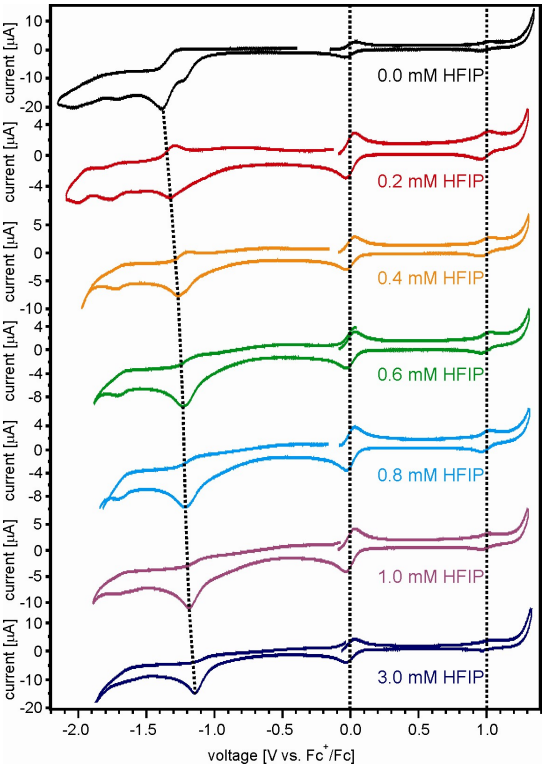

Figure 5. Cyclic voltammograms measured on the Ru-xy_1-AQ dyad in dry and deoxygenated CH_2Cl_2 in presence of increasing concentrations of hexafluoroisopropanol (from top to bottom) and in presence of 0.1 M $TBAPF_6$ electrolyte.

The reversible wave near 1.0 V vs. Fc^+/Fc is caused by the $Ru(bpy)_3^{3+/2+}$ couple.[26] Despite the low current associated with this particular wave, it is clear from Figure 5 that this redox potential is independent of the HFIP concentration (dashed vertical line on the right). In the series of voltammetry sweeps shown in Figure 5, reduction of AQ is not reversible. Therefore we use the current peak associated with AQ reduction as an indicator for the effect of HFIP on the $AQ/AQ^{\cdot-}$ reduction potential. This current peak potential shifts from -1.39 V vs. Fc^+/Fc in pure CH_2Cl_2 to -1.14 V vs. Fc^+/Fc in CH_2Cl_2 containing HFIP at 3 mM concentration; in Figure 5 this shift is illustrated by the left vertical dashed line. The pK_a value of the conjugate acid of $AQ^{\cdot-}$ is 5.3 in DMF while HFIP has pK_a = 17.9 in DMSO,[22, 46] hence protonation of anthraquinone monoanion by HFIP can be ruled out based on thermodynamic grounds. Consequently, following Gupta and Linschitz, we assign these potential shifts to changes in fast hydrogen-bonding equilibria which are closely coupled to reduction:[22]

$$AQ^{\cdot-} + n\,\text{HFIP} \leftrightarrows AQ^{\cdot-}\text{-HFIP}_n \qquad \text{(eq. 4)}$$

In the absorption titration of Figure 3 it was necessary to work with HFIP concentrations on the order of 0.5 M while for the cyclic voltammetry data in Figure 5 the main effect is observed between 0 and 3 mM. This observation suggests that hydrogen bonding to anthraquinone monoanion is significantly more important than hydrogen bonding to charge-neutral AQ, hence there may be binding of more than one HFIP molecule to a given $AQ^{\cdot-}$ species. This possibility is reflected by the number *n* in the chemical equilibrium of equation 4.

Gupta and Linschitz demonstrated that hydrogen bonding to benzoquinone monoanions can be evaluated quantitatively from cyclic voltammetry data. Specifically, it is possible to determine the equilibrium constant ($K_{eq}^{(AQ\text{-}\cdot)}$) associated with the chemical reaction of equation 4 from the experimentally observed shifts in AQ reduction potentials (ΔE_{red}) using the following expression:[22, 47]

$$\Delta E_{red} = n \cdot (R \cdot T/F) \cdot \ln([\text{HFIP}]) + (R \cdot T/F) \cdot \ln(K_{eq}^{(AQ\text{-}\cdot)}) \qquad \text{(eq. 5)}$$

In equation 5, R is the gas constant, T the temperature, and *F* the Faraday constant. ΔE_{red} is the difference between the electrochemical potentials for AQ reduction at a given HFIP concentration above 0.0 mM and the potential at [HFIP] = 0 mM. The factor *n* represents the number of hydrogen-bonded HFIP molecules per $AQ^{\cdot-}$ monoanion. Figure 6 shows a plot of the experimentally determined ΔE_{red}-values versus log([HFIP]).

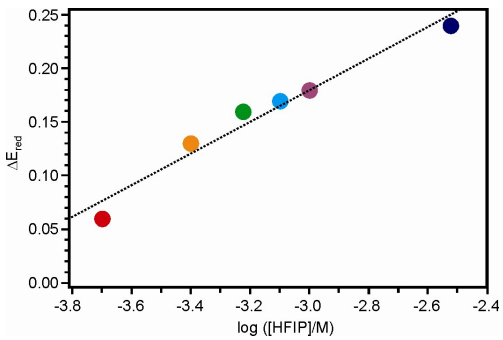

Figure 6. Plot of the shift in AQ/AQ^{-} reduction potential (ΔE_{red}) within increasing HFIP concentration as observed experimentally in the data from Figure 5 (with the same color code); see text for exact definition of ΔE_{red}. This semilogarithmic plot serves to determine $K_{eq}^{(AQ-)}$ according to equation 5.

As expected from equation 5, the data points fall (nearly) onto a straight line. A linear regression fit yields a slope of 0.15 V and an intercept of 0.62 V (R^2 = 0.9815). According to equation 5 the slope corresponds to $2.3 \cdot n \cdot (R \cdot T/F)$, and from this we obtain n ≈ 2.5. The equilibrium constant can be estimated from the intercept, and this gives $K_{eq}^{(AQ-)} \approx 3.6 \cdot 10^4\ M^{-2.5}$. $K_{eq}^{(AQ-)}$ represents a cumulative association constant for the binding of 2.5 HFIP molecules per anthraquinone monoanion. When calculating a mean association constant per individual HFIP molecule, one obtains $(3.6 \cdot 10^4\ M^{-2.5})^{1/2.5} = 66\ M^{-1}$, which is in good agreement with the values found by Gupta, Linschitz, and others for a variety of quinone monoanions in benzonitrile solution.[22, 47] Thus, we may conclude that reduction of AQ to

$AQ^{\bullet-}$ increases the number of HFIP molecules which are hydrogen-bonded to a given anthraquinone moiety of Ru-xy_1-AQ from 1 to 2.5,[48] and at the same time the (mean) binding constant per HFIP molecule increases from ~1 M^{-1} to ~66 M^{-1}. In other words, there are not only more HFIP molecules that bind to $AQ^{\bullet-}$ than to charge-neutral AQ, but the individual HFIP molecules also bind significantly more tightly (Scheme 2a).

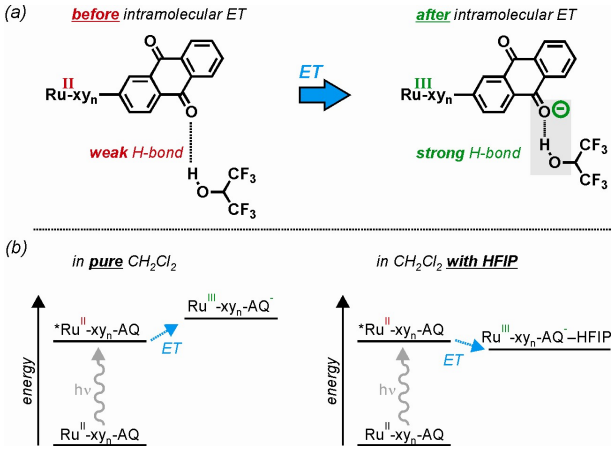

Scheme 2. (a) Hydrogen-bonding between anthraquinone and hexafluoroisopropanol before and after intramolecular Ru-to-AQ electron transfer. (b) Energetics for photoinduced Ru-to-AQ electron transfer in pure CH_2Cl_2 (left) and in CH_2Cl_2 with 1 M HFIP (right).

Influence of HFIP on photoinduced electron transfer in the Ru-xy_n-AQ molecules. When adding HFIP to a dichloromethane solution of Ru-xy_1-AQ the reduction of AQ becomes easier, while the oxidation of the $Ru(bpy)_3^{2+}$ unit stays essentially unaffected (Figure 5). Consequently, in presence of HFIP there is more driving force for intramolecular electron transfer between photoexcited $Ru(bpy)_3^{2+}$ and AQ. Based on equation 1 and E_{red} = -1.14 V vs. Fc^+/Fc (that is the value determined for [HFIP] = 3 mM), one estimates ΔG_{ET} = -0.12 eV. In other words, the thermodynamics for photoinduced electron transfer change from slightly endergonic in absence of HFIP (+0.09 eV; Table 1) to slightly exergonic (Scheme 2b).[49] One might therefore expect the ^{3}MLCT excited state of the $Ru(bpy)_3^{2+}$ unit in the Ru-

xy_n-AQ dyads to be quenched by intramolecular electron transfer when HFIP is added to the CH_2Cl_2 solution. The data in Figure 7c (left bottom panel) suggests that this is indeed the case: In deoxygenated CH_2Cl_2 containing no HFIP the luminescence intensity at 610 nm decays with a lifetime of 929 ns. Upon addition of increasing amounts of HFIP the lifetime gradually shortens until it reaches a value of 249 ns at an HFIP concentration of 1.0 M. At HFIP concentrations above 0.4 M there are very minor deviations from strictly single-exponential luminescence decay behavior (red, purple and violet traces in Figure 7c/7d), which are possibly due to static luminescence quenching.[50] However, these deviations occur after more than 99% of the initial intensity have decayed and are therefore so minor that analysis of the respective data in terms of single-exponential decay curves remains meaningful.

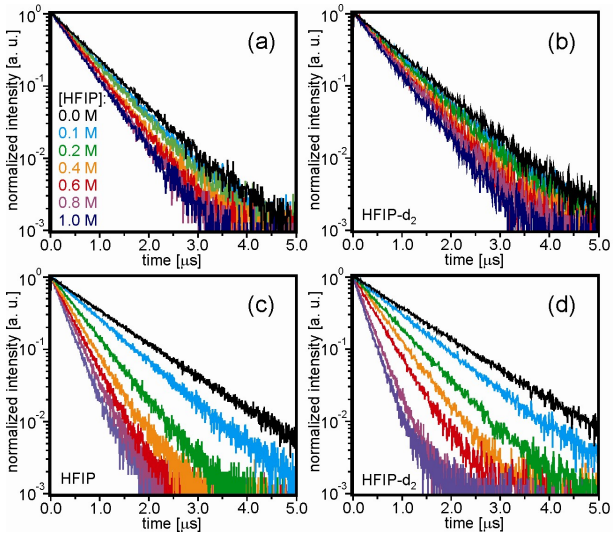

Figure 7. ^{3}MLCT luminescence decays of the $Ru(bpy)_3^{2+}$ unit in two different compounds in deoxygenated CH_2Cl_2 in presence of increasing concentrations of HFIP; the concentration of the emissive compounds was ~10^{-5} M; in all cases the HFIP concentration was as indicated in the legend in panel (a). Excitation occurred at 450 nm with laser pulses of 10 ns width, detection was at 610 nm. The emissive samples were: (a) isolated $Ru(bpy)_3^{2+}$ complex in presence of ordinary HFIP; (b) isolated $Ru(bpy)_3^{2+}$ complex in presence of deuterated HFIP (HFIP-d_2); (c) Ru-xy_1-AQ in presence of ordinary

HFIP; (c) Ru-xy$_1$-AQ in presence of deuterated HFIP (HFIP-d$_2$). In all cases the data was normalized to an initial intensity of 1 (in arbitrary units).

Transient absorption spectroscopy has the potential to provide unambiguous evidence for electron transfer photoproducts, and hence we attempted to detect $AQ^{\bullet-}$ or $Ru(bpy)_3^{3+}$ using this particular technique. $AQ^{\bullet-}$ is known to exhibit characteristic absorption bands around 390 nm and 570 nm,[16-17, 20, 51] while the formation of $Ru(bpy)_3^{3+}$ from $Ru(bpy)_3^{2+}$ should cause a bleaching of the ^{1}MLCT absorption around 450 nm.[52-53] However, our efforts to detect either $Ru(bpy)_3^{3+}$ or $AQ^{\bullet-}$ by nanosecond transient absorption spectroscopy have been unsuccessful, presumably due to rapid disappearance of these species by thermal electron transfer in the opposite sense. Indeed, this scenario is not uncommon in the field of photoinduced electron transfer,[5] including previously investigated systems with $Ru(bpy)_3^{2+}$ and benzoquinone redox partners.[54] In the absence of direct evidence for electron transfer photoproducts, the observation of luminescence quenching must be interpreted with care. In principle, the ^{3}MLCT excited-state of $Ru(bpy)_3^{2+}$ could also be quenched by triplet-triplet energy transfer to any of the attached molecular components. However, free anthraquinone has its lowest triplet excited state at 2.69 eV,[55] while the ^{3}MLCT state of $Ru(bpy)_3^{2+}$ is at 2.12 eV.[26] Thus, $Ru(bpy)_3^{2+}$ -to-AQ triplet-triplet energy transfer is estimated to be endergonic by more than 0.5 eV, and consequently this becomes a very unlikely excited-state quenching mechanism. Moreover, if populated, the lowest triplet excited state of the AQ unit should be rather easily detectable by transient absorption spectroscopy because one would expect it to have a lifetime well beyond 100 ns – similar to the lowest triplet excited states of anthracene or pyrene which can be populated by triplet-triplet energy transfer from $Ru(bpy)_3^{2+}$ units.[56-60] Given the unfavorable thermodynamics and the absence of long-lived transient absorption features after $Ru(bpy)_3^{2+}$ excitation, triplet-triplet energy transfer is ruled out as an efficient quenching source.

However, when relying exclusively on luminescence decay data for determining the effect of HFIP addition to CH_2Cl_2 solutions of the Ru-xy$_n$-AQ molecules, one must also examine what effect HFIP might have on the inherent $Ru(bpy)_3^{2+}$ excited-state lifetime in the isolated complex. The result from

this investigation is shown in Figure 7a (upper left panel). It turns out that the $Ru(bpy)_3^{2+}$ luminescence decays faster when HFIP is added: In deoxygenated pure CH_2Cl_2 the lifetime is 659 ns, in presence of 1.0 M HFIP it shortens to 455 ns. This excited-state lifetime shortening is likely due to more efficient nonradiative relaxation in presence of HFIP: High-frequency vibrations such as the O-H stretch in HFIP are known to be efficient luminescence killers.[61] However, this lifetime shortening is clearly less pronounced than in the case of Ru-xy_1-AQ (Figure 7c), where the lifetime decreases by a factor of 3.7 between 0.0 M and 1.0 M HFIP in CH_2Cl_2. In other words, in Ru-xy_1-AQ addition of HFIP enables an additional nonradiative excited-state deactivation process which is absent in isolated $Ru(bpy)_3^{2+}$, and it appears plausible to attribute the additional quenching to photoinduced electron transfer to AQ – particularly in view of our driving-force estimates from above which predict a change from ΔG_{ET} = +0.09 eV in absence of HFIP to ΔG_{ET} = -0.12 eV in presence of small amounts of HFIP (Scheme 2b).

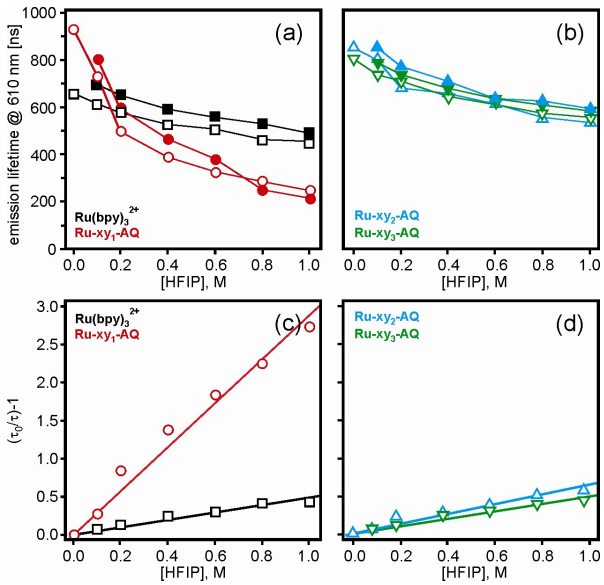

Figure 8. (a) ^{3}MLCT luminescence lifetime of isolated $Ru(bpy)_3^{2+}$ (black trace) and Ru-xy_1-AQ (red trace) in deoxygenated CH_2Cl_2 as a function of HFIP concentration. Open squares / circles: data measured using un-deuterated HFIP; filled squares / circles: data measured using HFIP-d_2. (b) ^{3}MLCT

luminescence lifetime of Ru-xy$_2$-AQ (blue trace) and Ru-xy$_3$-AQ (green trace) in deoxygenated CH_2Cl_2 as a function of HFIP concentration. Open triangles: data measured using ordinary HFIP; filled triangles: data obtained using HFIP-d$_2$. (c) Stern-Volmer plot based on the luminescence lifetime data from panel (a); (d) Stern-Volmer plot of the based on the luminescence lifetime data from panel (b). Linear regression fits were forced to pass through the origin and yield the quenching constants (k_Q) reported in Table 2. τ_0 is the luminescence lifetime in absence of HFIP, τ the lifetime in presence of variable concentrations of HFIP. Excitation was at 450 nm, detection at 610 nm in all cases.

Analogous luminescence lifetime measurements were performed with the Ru-xy$_2$-AQ and Ru-xy$_3$-AQ molecules (for raw data analogous to those of Figure 7 see Supporting Information), but in both samples the effect of HFIP is virtually the same as that in the case of the $Ru(bpy)_3^{2+}$ reference complex: Figure 8b plots the luminescence lifetimes of the two longer dyads in deoxygenated CH_2Cl_2 as a function of HFIP concentration (blue and green traces), and in both cases the behavior is similar to that of $Ru(bpy)_3^{2+}$ (black trace in Figure 8a).

Thus, photoinduced intramolecular electron transfer appears to be inefficient in the longer dyads. Electron transfer rates were found to drop off by factors of 1 – 1.4 per 1-Å distance increase in oligo-*p*-xylene bridged donor-acceptor systems (β = 0.52 Å^{-1} – 0.77 Å^{-1}),[27, 62-63] hence electron transfer in the longer dyads is expected to be slower by factors of 4 – 6 (Ru-xy$_2$-AQ) and 9 – 12 (Ru-xy$_3$-AQ) compared to Ru-xy$_1$-AQ. Apparently, this is sufficient to make photoinduced electron transfer uncompetitive with other ^{3}MLCT deactivation processes.

Table 2. Slopes determined from linear regression fits to the Stern-Volmer plots in Figure 8c/8d (K_{SV}) and bimolecular rate constants (k_Q) for $Ru(bpy)_3^{2+}$ ^{3}MLCT quenching in deoxygenated CH_2Cl_2 in presence of HFIP. k_{ET} is a rate constant for intramolecular electron transfer from the photoexcited $Ru(bpy)_3^{2+}$ moiety to AQ which is hydrogen-bonded to HFIP.

species	K_{SV} [M^{-1}]	k_Q [$M^{-1}s^{-1}$]	k_{ET} [s^{-1}]
$Ru(bpy)_3^{2+}$	0.50	$7.6 \cdot 10^5$	
Ru-xy_1-AQ	2.90	$4.4 \cdot 10^6$	$4.4 \cdot 10^6$
Ru-xy_2-AQ	0.55	$8.3 \cdot 10^5$	
Ru-xy_3-AQ	0.50	$7.6 \cdot 10^5$	

Figure 8c/8d shows Stern-Volmer plots based on the lifetime data from Figure 8a/8b. Linear regression fits to the four individual data sets yields slopes ranging from 0.50 M^{-1} to 2.90 M^{-1} (K_{SV} values in Table 2). At first glance, the K_{SV}-values of the Ru-xy_n-AQ molecules might be interpreted as equilibrium constants for the formation of hydrogen-bonded adducts between HFIP and the AQ moieties of the dyads. The order of magnitude of the K_{SV}-values is certainly consistent with the equilibrium constant determined from the data in Figure 3 ($K_{eq}^{(AQ)} \approx 1\ M^{-1}$). However, for the $Ru(bpy)_3^{2+}$ reference complex this interpretation does not appear to make much sense, and further it is not obvious why equilibrium constants would decrease from 2.90 M^{-1} to 0.50 M^{-1} between Ru-xy_1-AQ and Ru-xy_3-AQ. Thus, it appears meaningful to calculate rate constants for bimolecular excited-state quenching (k_Q) in presence of HFIP. Based on τ_0 = 659 ns for the $Ru(bpy)_3^{2+}$ ^{3}MLCT lifetime (see above), we obtain the k_Q-values reported in the third column of Table 2. These quenching constants vary in the narrow range from $7.6 \cdot 10^5$ $M^{-1}s^{-1}$ to $8.3 \cdot 10^5$ $M^{-1}s^{-1}$ between $Ru(bpy)_3^{2+}$, Ru-xy_2-AQ and Ru-xy_3-AQ, while for Ru-xy_1-AQ one finds $k_Q = 4.4 \cdot 10^6$ $M^{-1}s^{-1}$, i. e., a rate constant that is roughly a factor of 5 above all other k_Q values. From the discussion above we conclude that in the case of the reference complex and the two longer dyads (n = 2, 3) quenching by HFIP occurs directly at the $Ru(bpy)_3^{2+}$ unit through increasingly efficient multiphonon relaxation, whereas in the case of Ru-xy_1-AQ a significant extent of quenching occurs indirectly through increasingly efficient intramolecular electron transfer from the $Ru(bpy)_3^{2+}$ ^{3}MLCT excited state to AQ (Scheme 2b).[64] For the Ru-xy_1-AQ dyad it appears possible to estimate a rate constant for intramolecular ruthenium-to-anthraquinone electron transfer.[65,50] Based on $k_Q = 4.4 \cdot 10^6$ $M^{-1}s^{-1}$ (Table 2) and $K_{eq}^{(AQ)} = 1\ M^{-1}$ (data from Figure 3), one obtains $k_{ET} = 4.4 \cdot 10^6\ s^{-1}$. This value is

roughly a factor of 3 larger than the inherent ^{3}MLCT decay rate constant ($(659\ ns)^{-1} = 1.5 \cdot 10^6\ s^{-1}$), consistent with the observation of significant luminescence quenching in this particular dyad in presence of HFIP.

As seen above, AQ reduction in presence of HFIP is associated with a significant change in hydrogen-bonding equilibrium. An interesting question is whether in the case of intramolecular photoinduced electron transfer in Ru-xy$_1$-AQ the change in equilibrium occurs after the electron transfer event or whether there is a concerted overall reaction mechanism.[11] Scheme 3 illustrates the possible reaction pathways: Initially, one HFIP molecule is weakly ($K_a = 1\ M^{-1}$) hydrogen-bonded to charge-neutral AQ (upper left panel). Intramolecular electron transfer transiently produces Ru(III) and AQ^-, and immediately after electron transfer the hydrogen-bonding situation may still be the same as that before the photoreaction (upper right panel). Additional and stronger hydrogen bonds ($K_a = 3.6 \cdot 10^4\ M^{-2.5}$) can subsequently be formed to the AQ^- photoproduct (lower right panel). Aside from this stepwise reaction pathway along the upper right corner of Scheme 3, concerted reaction along the diagonal from the upper left directly to the lower right is conceivable. This latter process is conceptually similar to concerted proton-electron transfer (CPET),[66-67] with the important difference that some finite proton density rather than a full proton is transferred between HFIP and AQ. In the field of proton-coupled electron transfer (PCET) it is common to distinguish CPET events from stepwise electron transfer, proton transfer processes by exploring H/D kinetic isotope effects (KIEs).[66-70] A KIE ≥ 2 is commonly considered indicative of CPET, although the magnitude of a KIE depends on many parameters and is very difficult to predict.[71-72] In an attempt to shed some light on the reaction pathway of our Ru-xy$_1$-AQ system, we measured the ^{3}MLCT luminescence decays of this species in presence of deuterated HFIP. The results of these measurements are shown in Figure 7d and are found to differ in no significant way from the results obtained with ordinary HFIP (Figure 7c). Likewise, the luminescence of the isolated $Ru(bpy)_3^{2+}$ complex is virtually unaffected by deuteration of HFIP (Figure 7b).

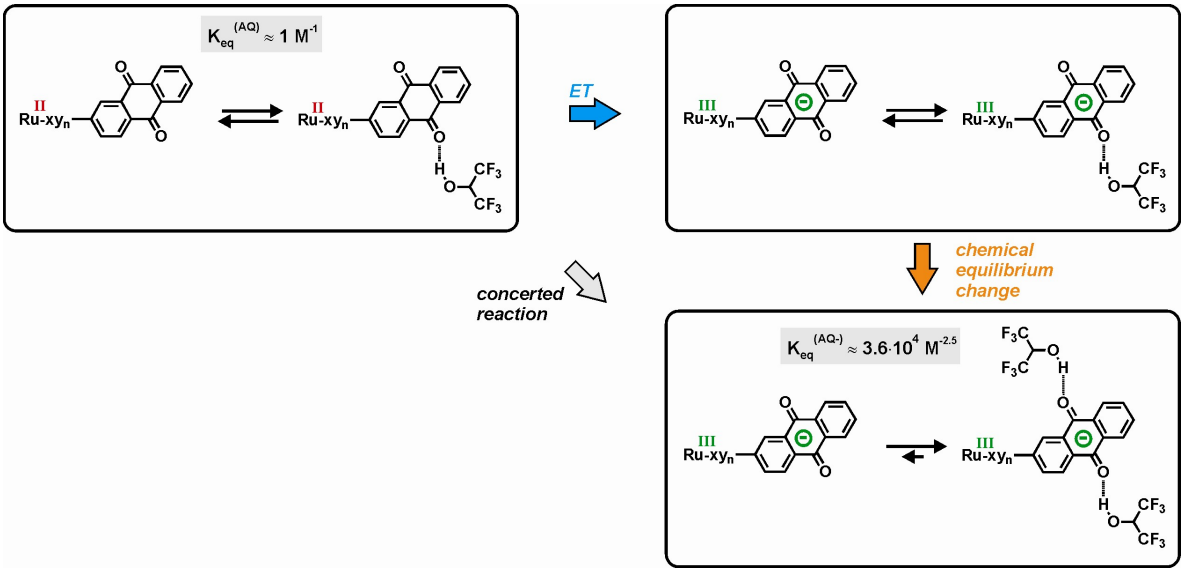

Scheme 3. Possible reaction pathways for intramolecular Ru-to-AQ electron transfer and hydrogen-bonding re-equilibration with HFIP upon AQ reduction: Stepwise pathway along the upper right corner, concerted pathway along the diagonal from the upper left to the lower right.

The insensitivity of the Ru-xy$_1$-AQ luminescence kinetics to HFIP deuteration suggests than the rate-determining excited-state quenching step is insensitive to proton motion, hence reaction along the upper right corner of Scheme 3 appears more plausible than a concerted process along the diagonal. A stepwise electron transfer, hydrogen-bond rearrangement reaction sequence does also make sense in view of the comparatively large concentrations of HFIP which are necessary to induce noticeable excited-state quenching.

A final technical point in this section concerns the minor deviations from strictly single exponential luminescence decay behavior in some of the data of Figure 7.

Photoinduced electron transfer in the Ru-xy$_n$-AQ molecules in acetonitrile-water mixtures. Water is known to be a good hydrogen-bond donor to benzoquinone mono- and dianions,[73-74] and therefore we decided to explore the influence of water on the intramolecular electron transfer kinetics in

the Ru-xy$_n$-AQ molecules. For solubility reasons it is necessary to work with acetonitrile-water mixtures rather than pure water. As seen from Figure 9b, already in pure CH_3CN the ^{3}MLCT luminescence of Ru-xy$_1$-AQ decays significantly more rapidly (green trace) than in pure CH_2Cl_2 (black trace), while in isolated Ru(bpy)$_3^{2+}$ (Figure 9a) the luminescence kinetics in these two solvents are much more similar to each other. This observation suggests that intramolecular electron transfer in Ru-xy$_1$-AQ is more efficient in the more polar CH_3CN solvent than in CH_2Cl_2, and this interpretation is supported by cyclic voltammetry: Figure 2 shows that AQ is reduced more easily in CH_3CN than in CH_2Cl_2 while Ru(II) is oxidized more readily. Consequently, based on equation 1 there is about 0.06 eV more driving force for photoinduced intramolecular electron transfer in CH_3CN than in CH_2Cl_2 (5th and 6th column of Table 1).

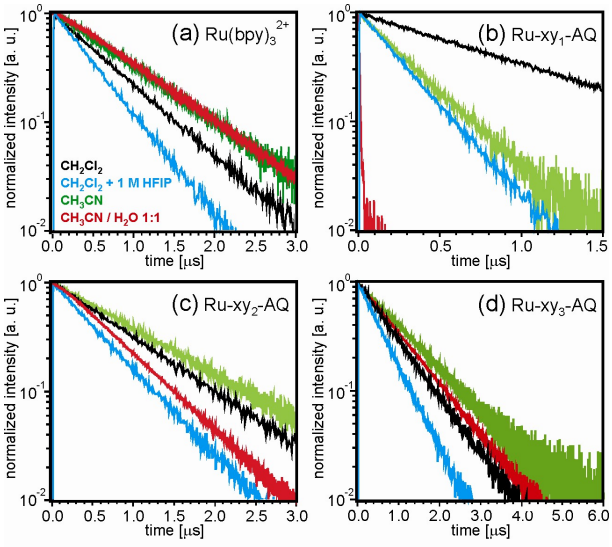

Figure 9. ^{3}MLCT luminescence decays at 610 nm of various compounds in different deoxygenated solvents: (a) isolated Ru(bpy)$_3^{2+}$ reference complex; (b) Ru-xy$_1$-AQ; (c) Ru-xy$_2$-AQ; (b) Ru-xy$_3$-AQ. The solvents were as indicated by the legend in panel (a); a consistent color code was used throughout all four panels. Excitation occurred at 450 nm with 10-ns laser pulses (using the Edinburgh Instruments apparatus) in all cases except for the Ru-xy$_1$-AQ decay in CH_3CN-H_2O (red trace in panel (b)). For this specific decay, the Fluorolog322 instrument with TCSPC option and a Nanoled excitation source (407

nm) was used. The initial intensity measured immediately after the excitation pulse was normalized to 1 (in arbitrary units) in all cases.

All three Ru-xy$_n$-AQ dyads exhibit similar redox potentials (Table 1 and CV data in the Supporting Information), and consequently the driving-force for intramolecular electron transfer (ΔG_{ET}) is similar in all three cases. However, the ^{3}MLCT decays of the longer dyads Ru-xy$_2$-AQ (Figure 9c) and Ru-xy$_3$-AQ (Figure 9d) are similar in CH_3CN (green traces) and CH_2Cl_2 (black traces), indicating that intramolecular electron transfer in the two longer dyads is uncompetitive with other excited-state deactivation processes even in the more polar CH_3CN solvent.

Table 3. Lifetimes of the $Ru(bpy)_3^{2+}$ ^{3}MLCT excited state in various (deoxygenated) solvents as determined from the luminescence intensity decay at 610 nm.

species	τ [ns] CH_3CN	τ [ns] CH_3CN -H_2O[a]	τ [ns] CH_3CN-D_2O[a]	τ [ns] CH_3CN-H_2O-HCl[b]	τ [ns] CH_3CN-D_2O-DCl[b]
$Ru(bpy)_3^{2+}$	866	930	1043	856	970
Ru-xy$_1$-AQ	300	7[c]	8[c]	6[c]	3[c]
Ru-xy$_2$-AQ	1023	665	772	544	618
Ru-xy$_3$-AQ	1111	938	1195	1005	1080

[a] 1:1 (v:v) solvent mixture at an apparent pH of 7. [b] 1:1 (v:v) solvent mixture at an apparent pH of 2. [c] Shorter decay components of biexponential fits to the experimental data in Fig. 10. The slower decay component is on the order of 900 ns in all cases and is attributed to traces of comparatively strongly emissive $Ru(bpy)_3^{2+}$ impurities (complexes without attached AQ quencher). Excitation wavelengths were 407 nm for lifetimes shorter than 15 ns (Fluorolog322 instrument), and 450 nm for lifetimes longer than 15 ns (Edinburgh Instruments apparatus). Indicated pH values reflect the pH value of the water used for preparing the 1:1 CH_3CN/H_2O mixtures.

For the solvent change from pure acetonitrile to 1:1 (v:v) CH_3CN-H_2O mixtures, equation 1 predicts another slight increase in driving-force for intramolecular Ru-to-AQ electron transfer (last column in

Table 1) caused by the associated increase of the dielectric constant from 35.94 to 55.7.[32, 35] Although this increase in ΔG_{ET} is weaker than that associated with the change from CH_2Cl_2 to CH_3CN, the luminescence decays of the dyads (but not those of the reference complex) are much more sensitive to the change from pure acetonitrile to the CH_3CN-H_2O mixture: In Ru-xy_1-AQ (Figure 9b) the luminescence decays almost two orders of magnitude more rapidly in CH_3CN-H_2O (red trace) than in pure CH_3CN (green trace): As seen from Table 3, the ^{3}MLCT excited-state lifetime decreases from 300 ns to 7 ns. It is obvious from Figure 9b that this change in lifetime when going from CH_3CN (green trace) to CH_3CN-H_2O (red trace) is much more dramatic than that associated with the change from pure CH_2Cl_2 (black trace) to 1.0 M HFIP in CH_2Cl_2 (blue trace).

Even in the Ru-xy_2-AQ dyad (Figure 9c) there is evidence for additional excited-state quenching as the ^{3}MLCT lifetime shortens from 1023 ns (in deoxygenated CH_3CN) to 665 ns (in deoxygenated 1:1 (v:v) CH_3CN-H_2O). Only the luminescence kinetics of the Ru-xy_3-AQ dyad and those of the $Ru(bpy)_3^{2+}$ reference complex remain essentially unaffected by this particular solvent change. Similar to what was noted above for the dichloromethane studies, transient absorption experiments performed on CH_3CN-H_2O solutions of our dyads failed to provide direct spectroscopic evidence for Ru(III) or AQ^- photoproducts, hence the luminescence quenching data must remain our only piece of (indirect) evidence for photoinduced electron transfer. In situations in which the temporal build-up of photoproducts cannot be monitored directly, it is common to estimate electron (or energy) transfer rate constants from equation 6.[75-76]

$$k_{ET} = \tau_{dyad}^{-1} - \tau_{ref}^{-1} \qquad \text{(eq. 6)}$$

Using as τ_{dyad} values the Ru-xy_n-AQ lifetimes from Table 3 and as τ_{ref} values the $Ru(bpy)_3^{2+}$ lifetime under identical conditions, one obtains the electron transfer rate constants (k_{ET}) given in Table 4. In pure CH_3CN, $k_{ET} = (2.2\pm0.4)\cdot10^6$ s^{-1} for Ru-xy_1-AQ (the uncertainty is determined by the 10% accuracy of our lifetime measurements), while in CH_3CN:H_2O k_{ET} is on the order of 10^8 s^{-1} for the shortest dyad and

k_{ET} = (4.3±2.5)·10^5 s^{-1} for Ru-xy_2-AQ. Given an inherent excited-state deactivation rate constant of 1.1·10^6 s^{-1} for the isolated $Ru(bpy)_3^{2+}$ complex, electron transfer in Ru-xy_2-AQ is just barely competitive with other excited-state relaxation processes.

The large increase in k_{ET} of Ru-xy_1-AQ between pure CH_3CN and CH_3CN-H_2O cannot be reconciled in a reasonable manner with the very small driving-force increase predicted by equation 1 (Table 1). Due to solubility issues we have been unable to determine the redox potentials of the ruthenium and AQ components of our dyads in aqueous solution or in CH_3CN-H_2O, hence cannot exclude the possibility that by basing our ΔG_{ET} estimates on potentials determined in acetonitrile, we are actually underestimating the driving-force for intramolecular electron transfer in the CH_3CN-H_2O solvent mixture. It appears plausible that the reduction of AQ is facilitated by hydrogen-bond donation from water and that this effect causes the large increase in intramolecular electron transfer rates in Ru-xy_1-AQ and Ru-xy_2-AQ.

Table 4. Rate constants for $Ru(bpy)_3^{2+}$ ^{3}MLCT excited-state quenching by electron transfer to AQ as estimated with equation 6 based on the luminescence decay data from Table 3. The luminescence lifetime of the unsubstituted $Ru(bpy)_3^{2+}$ complex was used as a τ_{ref} value.

species	k_{ET} [s^{-1}] CH_3CN	k_{ET} [s^{-1}] CH_3CN-H_2O
Ru-xy_1-AQ	(2.2±0.4)·10^6	(1.4±0.3)·10^8
Ru-xy_2-AQ	< 10^5	(4.3±2.5)·10^5
Ru-xy_3-AQ	< 10^5	< 10^5

The conjugate acid of anthraquinone has pK_a = -8.2 in H_2O,[77] hence the AQ component in the Ru-xy_n-AQ molecules cannot be protonated by water (pK_a = 15.7) or H_3O^+ (pK_a = -1.7). However, the conjugate acid of anthraquinone monoanion has pK_a = 5.3 in aqueous solution,[46] and hence it appears plausible

that once AQ^- is formed, it is protonated by H_3O^+. In order to elucidate whether this has any influence on the rate-determining excited-state deactivation step, we measured the luminescence lifetimes of the Ru-xy_n-AQ dyads and the $Ru(bpy)_3^{2+}$ reference complex in CH_3CN-H_2O mixtures with apparent pH values of 7 and 2.[78] As seen from Figure 10 and Table 3, the increase in H_3O^+ concentration by five orders of magnitude has no effect on the ^{3}MLCT lifetime, and we conclude that proton transfer, if occurring at all, has no influence on the rate-determining electron transfer step. Thus, if an overall PCET process occurs, it is likely to occur through a sequence of electron transfer and proton transfer steps rather than concerted proton-electron transfer (CPET). The absence of a kinetic isotope effect (derived from comparison of lifetime measurements in CH_3CN:H_2O and CH_3CN:D_2O both at pH 7 and pH 2, Figure 10 and Table 3) is consistent with this interpretation.

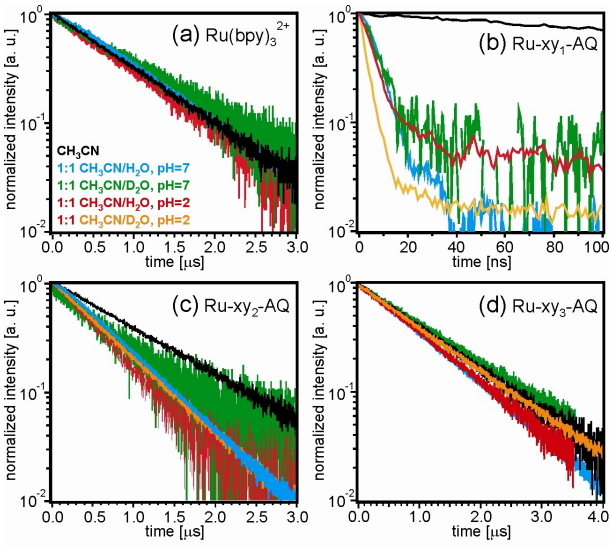

Figure 10. ^{3}MLCT luminescence decays at 610 nm of various compounds in different deoxygenated solvents: (a) isolated $Ru(bpy)_3^{2+}$ reference complex; (b) Ru-xy_1-AQ; (c) Ru-xy_2-AQ; (b) Ru-xy_3-AQ. The solvents were as indicated by the legend in panel (a); a consistent color code was used in all four panels; 1:1 ratios are in v:v; indicated pH values reflect the pH value of the water used for preparing the 1:1 CH_3CN/H_2O mixtures. Note the different time scales in the four different panels. The initial

intensity measured immediately after the excitation pulse was normalized to 1 (in arbitrary units) in all cases. Excitation wavelength was 450 nm in panels (a), (c), (d) and 407 nm for the data in panel (b). The decays measured on the Ru-xy$_1$-AQ sample are biexponential; the shorter decay component is attributed to the inherent ^{3}MLCT decay of this particular sample, while the longer decay component is on the order of 900 ns in all cases and is therefore attributed to minor Ru(bpy)$_3^{2+}$ impurities that are comparatively strongly emissive.

SUMMARY AND CONCLUSIONS

The rate of photoinduced intramolecular electron transfer in the Ru-xy$_1$-AQ dyad increases markedly upon addition of hydrogen bond donors that can bind to the anthraquinone unit. In dichloromethane, the experimental evidence is consistent with the binding of 1 HFIP molecule per charge-neutral AQ moiety, the association constant (K_a) is only on the order of 1 M^{-1}. Upon reduction to AQ^- there are on average 2.5 hydrogen-bonded HFIP molecules per AQ unit, and the K_a value increases to $3.6 \cdot 10^4$ $M^{-2.5}$ (or 66 M^{-1} per HFIP molecule). Thermodynamically, the net result of hydrogen bonding between HFIP and AQ is an increase in the driving-force for intramolecular Ru-to-AQ electron transfer, manifesting itself in the abovementioned acceleration of reaction kinetics – at least in the shortest of the three dyads considered here. Comparative time-resolved experiments performed with ordinary and deuterated HFIP suggest that photoinduced intramolecular electron transfer and the change in hydrogen-bonding equilibrium occur in stepwise (rather than concerted) manner. When replacing CH_2Cl_2 by the more polar CH_3CN solvent, photoinduced intramolecular electron transfer is accelerated as well because of the greater ease of AQ reduction and Ru(bpy)$_3^{2+}$ oxidation in CH_3CN relative to CH_2Cl_2. A change from pure acetonitrile to 1:1 (v:v) CH_3CN-H_2O leads to an even more important increase of electron transfer rates, which is likely due to hydrogen-bonding of water molecules to AQ and $AQ^{\cdot-}$, similar to what could be elucidated in greater detail for the CH_2Cl_2-HFIP solvent system. In CH_3CN-H_2O there is the thermodynamic

possibility of an overall proton-coupled electron transfer reaction, but the experimental evidence (including lifetime measurements at different pH values in deuterated and non-deuterated solvents) is consistent with simple electron transfer in the rate-determining reaction step.

Thus, in presence of hydrogen-bond donors some of our Ru-xy$_n$-AQ dyads exhibit a variant of PCET: Hydrogen bonds are strengthened upon intramolecular electron transfer, implying that some finite proton density (rather than a full proton as in true PCET) is shifted from the hydrogen-bond donors towards the AQ electron acceptor. The experimental evidence suggests that in the specific case of our anthraquinone electron/proton acceptors the overall process takes place in consecutive electron transfer, hydrogen-bonding re-equilibration steps. This is similar to the redox chemistry of the quinone at the end of the electron transfer cascade in photosynthetic reaction centers of bacteria, where the first reduction step is a pure electron transfer reaction that is conformationally gated, and only subsequently there is fast proton transfer re-equilibration coupled to reduction by a second equivalent.[79]

EXPERIMENTAL SECTION

Commercially available chemicals were used as received without further purification. Where necessary, reactions were carried out under nitrogen using solvents which were dried by routine methods. Polygram SIL G/UV254 plates from Machery-Nagel were used for thin-layer chromatography. For preparative column chromatography, Silica Gel 60 from the same company was employed. ^{1}H and ^{13}C NMR spectroscopy was performed with a Bruker Avance DRX 300 or a Bruker B-ACS-120 spectrometer, using the deuterated solvent as the lock and residual solvent as an internal reference. Electron ionization mass spectrometry (EI-MS) was made with a Finnigan MAT8200 instrument, elemental analysis occurred on a Vario EL III CHNS analyzer from Elementar. Cyclic voltammetry was performed using a Versastat3-100 potentiostat from Princeton Applied Research equipped with a glassy carbon working electrode and a silver counter electrode. A silver wire also served as a quasi-reference electrode. Ferrocene (Fc) was used as an internal reference. Prior to voltage scans at rates of 100 mV/s,

nitrogen gas was bubbled through the dried solvent. The supporting electrolyte was a 0.1 M solution of tetrabutylammonium hexafluorophosphate. Optical absorption spectra were recorded on a Cary 300 spectrometer from Varian. Steady state luminescence spectra were measured on a Fluorolog-3 instrument (FL322) from Horiba Jobin-Yvon, equipped with a TBC-07C detection module from Hamamatsu. Time-resolved luminescence experiments occurred on the same Fluorolog-3 instrument equipped with the FL-1061PC Fluorohub for detection in TCSPC mode and a NanoLed-340L or a NanoLed-407 as pulsed excitation sources. Alternatively, an LP920-KS instrument from Edinburgh Instruments, equipped with an R928 photomultiplier and an iCCCD camera from Andor, was used for measurement of luminescence lifetimes longer than 15 ns. The excitation source was a Quantel Brilliant b laser equipped with an OPO from Opotek. Attempts to measure transient absorption were made using the same LP920-KS instrument. For all luminescence lifetime measurements, samples were deoxygenated thoroughly by bubbling nitrogen gas through the solutions. Solution infrared spectroscopy was performed on a ReactIR iC10 instrument with silver halide fiber optics from Mettler-Toledo.

ACKNOWLEDGMENT

Financial support from the Swiss National Science Foundation through grant number 200021-117578 and from the Deutsche Forschungsgemeinschaft through grant number INST186/872-1 is gratefully acknowledged.

SUPPORTING INFORMATION PARAGRAPH

Synthetic protocols and characterization data for the Ru-xy$_n$-AQ (n = 1 – 3) dyads and all intermediate reaction products. Cyclic voltammograms and additional luminescence lifetime data. This material is available free of charge via the Internet at http://pubs.acs.org.

REFERENCES

(1) Bertini, I.; Gray, H. B.; Stiefel, E. I.; Valentine, J. S., *Biological Inorganic Chemistry*. University Science Books: Sausalito, California, 2007.

(2) Renger, G.; Renger, T., *Photosynth. Res.* **2008,** *98*, 53-80.

(3) Alexov, E. G.; Gunner, M. R., *Biochemistry* **1999,** *38*, 8253-8270.

(4) Wasielewski, M. R., *Chem. Rev.* **1992,** *92*, 435-461.

(5) Balzani, V., *Electron transfer in chemistry*. VCH Wiley: Weinheim, 2001; Vol. 3.

(6) Hung, S. C.; Macpherson, A. N.; Lin, S.; Liddell, P. A.; Seely, G. R.; Moore, A. L.; Moore, T. A.; Gust, D., *J. Am. Chem. Soc.* **1995,** *117*, 1657-1658.

(7) Fukuzumi, S.; Okamoto, K.; Yoshida, Y.; Imahori, H.; Araki, Y.; Ito, O., *J. Am. Chem. Soc.* **2003,** *125*, 1007-1013.

(8) Biczok, L.; Linschitz, H., *J. Phys. Chem. A* **2001,** *105*, 11051-11056.

(9) Steinberg-Yfrach, G.; Liddell, P. A.; Hung, S. C.; Moore, A. L.; Gust, D.; Moore, T. A., *Nature* **1997,** *385*, 239-241.

(10) Gust, D.; Moore, T. A.; Moore, A. L.; Ma, X. C. C.; Nieman, R. A.; Seely, G. R.; Belford, R. E.; Lewis, J. E., *J. Phys. Chem.* **1991,** *95*, 4442-4445.

(11) Yago, T.; Gohdo, M.; Wakasa, M., *J. Phys. Chem. B* **2010,** *114*, 2476-2483.

(12) There is obviously a vast amount of work on photoinduced electron transfer in hydrogen-bonded donor-acceptor systems, but this is not directly relevant in the specific context of hydrogen-bond donation to quinone redox partners.

(13) Wenger, O. S., *Coord. Chem. Rev.* **2009,** *253*, 1439-1457.

(14) Frank, R.; Greiner, G.; Rau, H., *Phys. Chem. Chem. Phys.* **1999,** *1*, 3481-3490.

(15) Opperman, K. A.; Mecklenburg, S. L.; Meyer, T. J., *Inorg. Chem.* **1994,** *33*, 5295-5301.

(16) Mecklenburg, S. L.; McCafferty, D. G.; Schoonover, J. R.; Peek, B. M.; Erickson, B. W.; Meyer, T. J., *Inorg. Chem.* **1994,** *33*, 2974-2983.

(17) Lopéz, R.; Leiva, A. M.; Zuloaga, F.; Loeb, B.; Norambuena, E.; Omberg, K. M.; Schoonover, J. R.; Striplin, D.; Devenney, M.; Meyer, T. J., *Inorg. Chem.* **1999,** *38*, 2924-2930.

(18) Striplin, D. R.; Reece, S. Y.; McCafferty, D. G.; Wall, C. G.; Friesen, D. A.; Erickson, B. W.; Meyer, T. J., *J. Am. Chem. Soc.* **2004,** *126*, 5282-5291.

(19) Pellegrin, Y.; Forster, R. J.; Keyes, T. E., *Inorg. Chim. Acta* **2009,** *362*, 1715-1722.

(20) Hankache, J.; Wenger, O. S., *Chem. Commun.* **2011,** *47*, 10145-10147.

(21) Hankache, J.; Wenger, O. S., *Phys. Chem. Chem. Phys.* **2012,** *14*, 2685-2692.

(22) Gupta, N.; Linschitz, H., *J. Am. Chem. Soc.* **1997,** *119*, 6384-6391.

(23) Hensel, V.; Schlüter, A. D., *Liebigs Ann.* **1997**, 303-309.

(24) Hanss, D.; Wenger, O. S., *Eur. J. Inorg. Chem.* **2009**, 3778-3790.

(25) Walther, M. E.; Wenger, O. S., *ChemPhysChem* **2009,** *10*, 1203-1206.

(26) Roundhill, D. M., *Photochemistry and Photophysics of Metal Complexes*. Plenum Press: New York, 1994.

(27) Hanss, D.; Wenger, O. S., *Inorg. Chem.* **2008,** *47*, 9081-9084.

(28) Hanss, D.; Walther, M. E.; Wenger, O. S., *Coord. Chem. Rev.* **2010,** *254*, 2584-2592.

(29) Wenger, O. S., *Chem. Soc. Rev.* **2011,** *40*, 3538-3550.

(30) Goldsmith, R. H.; Sinks, L. E.; Kelley, R. F.; Betzen, L. J.; Liu, W. H.; Weiss, E. A.; Ratner, M. A.; Wasielewski, M. R., *Proc. Natl. Acad. Sci. U. S. A.* **2005,** *102*, 3540-3545.

(31) Weiss, E. A.; Ahrens, M. J.; Sinks, L. E.; Gusev, A. V.; Ratner, M. A.; Wasielewski, M. R., *J. Am. Chem. Soc.* **2004,** *126*, 5577-5584.

(32) Gagliardi, L. G.; Castells, C. B.; Rafols, C.; Roses, M.; Bosch, E., *J. Chem. Eng. Data* **2007,** *52*, 1103-1107.

(33) Weller, A., *Z. Phys. Chem.* **1982,** *133*, 93-98.

(34) Kilså, K.; Kajanus, J.; Macpherson, A. N.; Mårtensson, J.; Albinsson, B., *J. Am. Chem. Soc.* **2001,** *123*, 3069-3080.

(35) Gurzadyan, G. G.; Steenken, S., *Chem. Eur. J.* **2001,** *7*, 1808-1815.

(36) The middle term of eq. 1 cancels out here because es=eref`, but the complete eq. 1 will be necessary below.

(37) Lucarini, M.; Mugnaini, V.; Pedulli, G. F.; Guerra, M., *J. Am. Chem. Soc.* **2003,** *125*, 8318-8329.

(38) Biczok, L.; Gupta, N.; Linschitz, H., *J. Am. Chem. Soc.* **1997,** *119*, 12601-12609.

(39) Peters, R. H.; Sumner, H. H., *J. Chem. Soc.* **1953**, 2101-2110.

(40) Mataga, N.; Tsuno, S., *Bull. Chem. Soc. Jpn.* **1957,** *30*, 368-374.

(41) Mataga, N.; Tsuno, S., *Bull. Chem. Soc. Jpn.* **1957,** *30*, 711-715.

(42) Steed, J. W.; Atwood, J. L., *Supramolecular chemistry*. John Wiley&Sons., Ltd.: 2009.

(43) Pecile, C.; Lunelli, B., *J. Chem. Phys.* **1967,** *46*, 2109-2118.

(44) Büschel, M.; Stadler, C.; Lambert, C.; Beck, M.; Daub, J., *J. Electroanal. Chem.* **2000,** *484*, 24-32.

(45) White, A. J.; Wharton, C. W., *Biochem. J.* **1990,** *270*, 627-637.

(46) Babaei, A.; Connor, P. A.; McQuillan, A. J.; Umapathy, S., *J. Chem. Ed.* **1997,** *74*, 1200-1204.

(47) Ahmed, S.; Khan, A. Y.; Qureshi, R.; Subhani, M. S., *Russ. J. Electrochem.* **2007,** *43*, 811-819.

(48) Given the occurrence of isosbestic points in the absorption data of Figure 3, we assume that only two species occur: AQ and AQ with one hydrogen-bonded HFIP molecule.

(49) Note that the error associated with driving-force estimates based on eq. 1 is typically on the order of 0.1 eV.

(50) Concepcion, J. J.; Brennaman, M. K.; Deyton, J. R.; Lebedeva, N. V.; Forbes, M. D. E.; Papanikolas, J. M.; Meyer, T. J., *J. Am. Chem. Soc.* **2007,** *129*, 6968-6969.

(51) Lewis, F. D.; Thazhathveetil, A. K.; Zeidan, T. A.; Vura-Weis, J.; Wasielewski, M. R., *J. Am. Chem. Soc.* **2010,** *132*, 444-445.

(52) Sjödin, M.; Styring, S.; Åkermark, B.; Sun, L. C.; Hammarström, L., *J. Am. Chem. Soc.* **2000,** *122*, 3932-3936.

(53) Walther, M. E.; Wenger, O. S., *Inorg. Chem.* **2011,** *50*, 10901-10907.

(54) Borgström, M.; Johansson, O.; Lomoth, R.; Baudin, H. B.; Wallin, S.; Sun, L. C.; Åkermark, B.; Hammarström, L., *Inorg. Chem.* **2003,** *42*, 5173-5184.

(55) Turro, N. J., *Molecular Photochemistry*. New York, Amsterdam, 1967.

(56) Schanze, K. S.; MacQueen, D. B.; Perkins, T. A.; Cabana, L. A., *Coord. Chem. Rev.* **1993,** *122*, 63-89.

(57) Schoonover, J. R.; Dattelbaum, D. M.; Malko, A.; Klimov, V. I.; Meyer, T. J.; Styers-Barnett, D. J.; Gannon, E. Z.; Granger, J. C.; Aldridge, W. S.; Papanikolas, J. M., *J. Phys. Chem. A* **2005,** *109*, 2472-2475.

(58) Simon, J. A.; Curry, S. L.; Schmehl, R. H.; Schatz, T. R.; Piotrowiak, P.; Jin, X. Q.; Thummel, R. P., *J. Am. Chem. Soc.* **1997,** *119*, 11012-11022.

(59) Walther, M. E.; Wenger, O. S., *Dalton Trans.* **2008**, 6311-6318.

(60) Freys, J. C.; Wenger, O. S., *Eur. J. Inorg. Chem.* **2010**, 5509-5516.

(61) Brunold, T. C.; Güdel, H. U., *Inorganic Electronic Structure and Spectroscopy*. Wiley: New York, 1999; Vol. 1, p 259-306.

(62) Wenger, O. S., *Acc. Chem. Res.* **2011**, 25-35.

(63) Hanss, D.; Wenger, O. S., *Inorg. Chem.* **2009,** *48*, 671-680.

(64) In addition, there is of course direct quenching at the $Ru(bpy)_3^{2+}$ site as in all three other compounds.

(65) This is not an uncommon procedure, see for example refs.50 and 70.

(66) Huynh, M. H. V.; Meyer, T. J., *Chem. Rev.* **2007,** *107*, 5004-5064.

(67) Mayer, J. M., *Annu. Rev. Phys. Chem.* **2004,** *55*, 363-390.

(68) Hammarström, L.; Styring, S., *Energy Environ. Sci.* **2011,** *4*, 2379-2388.

(69) Costentin, C.; Robert, M.; Savéant, J.-M., *Acc. Chem. Res.* **2010,** *43*, 1019-1029.

(70) Bronner, C.; Wenger, O. S., *J. Phys. Chem. Lett.* **2012,** *3*, 70-74.

(71) Hammes-Schiffer, S., *Acc. Chem. Res.* **2009,** *42*, 1881-1889.

(72) Hammes-Schiffer, S.; Stuchebrukhov, A. A., *Chem. Rev.* **2010,** *110*, 6939-6960.

(73) Sinnecker, S.; Reijerse, E.; Neese, F.; Lubitz, W., *J. Am. Chem. Soc.* **2004,** *126*, 3280-3290.

(74) Lubitz, W.; Isaacson, R.; Flores, M.; Sinnecker, S.; Lendzian, F.; Feher, G., *Biophys. J.* **2002,** *82*, 478A-478A.

(75) Schlicke, B.; Belser, P.; De Cola, L.; Sabbioni, E.; Balzani, V., *J. Am. Chem. Soc.* **1999,** *121*, 4207-4214.

(76) Schanze, K. S.; Sauer, K., *J. Am. Chem. Soc.* **1988,** *110*, 1180-1186.

(77) Yamada, Y. Anti-Allergen Agent. 2010.

(78) Indicated pH values reflect the pH value of the water used for preparing the 1:1 CH_3CN/H2O mixtures.

(79) Warren, J. J.; Tronic, T. A.; Mayer, J. M., *Chem. Rev.* **2010,** *110*, 6961-7001.

SYNOPSIS TOC